Influence of spacer layer morphology on the exchange-bias properties of reactively sputtered Co/Ag multilayers

P. S. Normile,[1] J. A. De Toro,[1] T. Muñoz,[1] J. A. González,[1] J. P. Andrés,[1] P. Muñiz,[1] R. E. Galindo,[2] and J. M. Riveiro[1]
[1]*Departamento de Física Aplicada, Universidad de Castilla-La Mancha, 13071 Ciudad Real, Spain*
[2]*Instituto de Ciencias de Materiales, CSIC, E-28049 Madrid, Spain*
(Received 5 December 2006; revised manuscript received 16 July 2007; published 25 September 2007)

We have studied the magnetic properties of $[Ag(t_{Ag})/Co(1.2\ nm)]_{60}$ multilayers grown in an oxygen atmosphere. Partial oxidation of the Co layers results in the appearance of t_{Ag} dependent exchange-bias properties. A strong increase in the exchange-bias field H_E together with a significant reduction in the coercivity H_C are observed when t_{Ag} is decreased below $t^*_{Ag}=4$ nm, whereas these two parameters adopt approximately constant values for $t_{Ag}>t^*_{Ag}$. At t^*_{Ag}, a transition from continuous to islandlike silver layers (on reducing t_{Ag}) is signaled by electrical resistivity and x-ray reflectivity results. From magnetic hysteresis loops recorded at room temperature and magnetization curves, it is concluded that this transition induces a granular morphology in the Co regions, which are previously ($t_{Ag}>t^*_{Ag}$) plateletlike, and enhances the oxidized fraction of Co (f_{CoO}). The increase (decrease) in H_E (H_C) with reducing t_{Ag} below t^*_{Ag} is correlated to the increase in both the electrical resistivity and f_{CoO}. From the latter correlation, we infer that the higher degree of oxidation in the granular Co layers is associated with effectively thicker antiferromagnetic (CoO) regions than in the $t_{Ag}>t^*_{Ag}$ (continuous multilayer) case—with correspondingly higher magnetic anisotropy energies—which may account for both the enhancement in H_E and the reduction in H_C. In addition, our study provides information on the surfactant effect of O_2 in Ag sputter growth since the continuity thickness value ($t^*_{Ag}=4$ nm) is found to be lower than those previously reported in nonreactive sputtering of Ag.

DOI: 10.1103/PhysRevB.76.104430 PACS number(s): 75.75.+a, 75.30.Gw, 82.70.Uv

I. INTRODUCTION

Recent research into the phenomenon of unidirectional exchange anisotropy [exchange bias (EB)] presents a growing interest in the study of core-shell ferromagnetic-antiferromagnetic (FM-AFM) particles embedded in nonmagnetic (NM) media.[1–6] These studies, so far limited to the case of Co-CoO particles, have involved sample preparation by both sequential[1,3,4,6] and codeposition[2,5] of the magnetic and NM materials, with Al_2O_3 (Refs. 1, 3, 4, and 6) and Ag (Refs. 2 and 5) being used as the NM (matrix) materials. In the study by Skumyrev *et al.*,[1] EB (characterized by a hysteresis loop shift along the applied field axis) was not observed for the case of Co-CoO particles embedded in Al_2O_3, whereas increasing the in-plane concentration of these particles, in a subsequent study,[6] produced EB due to stabilization of AFM order in the thin ($\approx$1 nm) CoO shells provided by particle-particle contact. Similar connectivity arguments have been used to explain the EB in other Co-CoO/Al_2O_3 samples.[4] However, in another study on sequentially deposited Co-CoO/Al_2O_3, the absence of EB has been explained *not* by a lack of connectivity (and, hence, of stable AFM order) but rather by the relative sizes of the effective Zeeman (E_Z), AFM anisotropy (E_{AFM}), and FM-AFM exchange ($E_{FM\text{-}AFM}$) energies.[3] For the case of studies, by some of us, on codeposited Co/Ag, EB only appears beyond a certain minimum O_2 pressure in the sputtering chamber,[2] which may be related to a critical AFM shell thickness. A subsequent annealing study on such an EB-possessing, codeposited Co/Ag sample showed a decrease in the EB field H_E when the temperature is sufficiently high to cause Co-CoO particles to coalesce, which can be explained by the concomitant reduction in the FM-AFM interface area (per unit quantity of Co).[5] However, an explanation of the initial increase in H_E upon annealing is still lacking.

EB properties may thus be altered in a system of core-shell particles embedded in a NM matrix by varying (a) the density of particles and, hence, the degree of connectivity, for the case of thin ($\lesssim$1 nm) AFM shells,[4,6] (b) the relative thicknesses of the FM and AFM regions, in order to change the relative sizes of the energies E_Z, E_{AFM}, and $E_{FM\text{-}AFM}$ [Refs. 2 and 3], or (c) changing the FM-AFM interface area per unit quantity of the FM material.[5] Point (c) is, indeed, a specific case of point (b) since it is another way of expressing the relationship $H_E \propto 1/t_{FM}$, where t_{FM} is the effective size of the FM regions, which holds for the most simple model of EB (the Meiklejohn-Bean or MB model).[7,8] With regard to the influence of E_{AFM} on the EB field, Lund *et al.*[9] recently confirmed a generalized MB model[10] by their elegant experiments on simple FM-AFM bilayer systems.

In the present paper, we experimentally revise the above ideas in a nanostructured system where the morphology of the "Co+CoO" regions is made to vary from a case in which the FM (Co) regions are essentially granular to a case in which they are plateletlike by sequentially depositing critically thin layers of Co (in a reactive atmosphere) onto Ag layers of varying thickness and, consequently, different morphologies. Our expectation of the thickness dependence of the Ag morphology follows the work by Paje *et al.*[11] on the rf sputter growth of Ag *in the absence of oxygen*, where it is observed that when the nominal thickness of the deposited Ag (t_{Ag}) is below a *continuity limit* $t^*_{Ag}=6$ nm, discontinuous films are obtained, while $t_{Ag}>6$ nm results in continuous films. A consistent value of t^*_{Ag} may be inferred from the t_{Ag} dependence of electrical resistivity in studies of dc sputtered (in the absence of oxygen) Ag/$Co_{90}Fe_{10}$ multilayers.[12] A sec-

ondary result of the present paper, the main focus being on explaining the EB properties of the multilayers as t_{Ag} is varied, is that the oxygen present during sputtering reduces the value of t_{Ag}^{*}, an effect we ascribe to the surfactant role of oxygen in silver sputter growth.[13] The so-called "critically thin" Co layers deposited correspond to the minimum layer nominal thickness that gives rise to a measurable FM response in the most unfavorable case (multilayer with the most discontinuous Ag morphology) when deposited in the selected oxygen atmosphere. In this way, any possible effect of the changing Ag morphology (upon increasing t_{Ag}) on the structure and, hence, on the EB properties of the magnetic layers is expected to be most pronounced.

Section III is divided into two parts. The first part groups together all data (including magnetic characterization) that lead to a structural picture of the multilayers as a function of t_{Ag}. In the second part, the t_{Ag} dependence of the EB properties are presented and explained based on certain conclusions drawn in the first part.

II. EXPERIMENT

A series of multilayer samples, each comprising 60 Co/Ag bilayers, with Co layer nominal thickness $t_{Co}^{nom}=1.2$ nm (constant across the series) and Ag layer nominal thickness t_{Ag}, varying from 1.8 to 9.4 nm across the series, were synthesized by reactive rf magnetron sputter deposition onto water-cooled glass substrates using high purity Co and Ag cathodes equipped with computer-controlled shutters. Sputtering powers and their associated deposition rates were 20 W and 0.42 nm/s (Ag deposition) and 30 W and 0.17 nm/s (Co deposition). These rates were determined by measuring the thickness of relatively thick ($\approx$50 nm) films by grazing incidence x-ray reflectivity (GIXR). The oxygen pressure in the sputtering chamber was 2×10^{-5} mbar, a value for which EB was observed in codeposited Ag-Co samples,[2] as well as in Co-CoO composite films[14] (30 W being the power used for Co deposition in both Refs. 2 and 14). Additionally, working at this O_2 pressure, the silver growth (at 20 W) is assisted by the oxygen, which plays the role of a surfactant, and no Ag oxide phase is formed.[13] The Ar and residual pressures in the chamber were 3×10^{-3} and 2×10^{-7} mbar, respectively.

A commercial vibrating-sample magnetometer (VSM) was used to measure hysteresis loops at room temperature, up to a maximum field $H_{max}=15$ kOe, and the temperature dependence of the sample magnetic moment after field cooling (FC) in $H=100$ Oe and zero-field cooling (ZFC). Measurements on multilayers with $t_{Co}^{nom}=0.9$ nm and $t_{Ag}=1.8$ nm, i.e., the (expected) most discontinuous Ag case, showed no FM response, i.e., the deposited Co was completely oxidized. This justified the use of $t_{Co}^{nom}=1.2$ nm (across the series) as the so-called critical Co thickness. Values of the EB and coercive fields, H_E and H_C, were extracted from hysteresis loops measured at $T=80$ K—and with $H_{max}=50$ kOe—immediately following field cooling with $H=10$ kOe using a commercial superconducting quantum interference device magnetometer. The EB onset temperature (T_{OE}) was estimated from hysteresis loops with $H_{max}=10$ kOe (VSM), recorded around $T=220$ K after heating from the field-cooled state ($T=80$ K) in temperature increments of 20 K, performing a hysteresis loop (with $H_{max}=10$ kOe) after each increment.

Several techniques were employed for structural characterization of the multilayers. A conventional four-probe configuration, using gold coated pin contacts, was used to measure the room temperature electrical resistivity of the multilayers (current parallel to the substrate surface). X-ray reflectivity (GIXR) and diffraction measurements were made in a specular (θ-2θ) geometry using a commercial diffractometer (Philips X'pert) employing Cu $K\alpha$ radiation. Glow discharge optical emission spectroscopy (GDOES) analysis was carried out using a Jobin Yvon rf GD Profiler equipped with a 4 mm diameter anode and operating at a typical radio frequency discharge pressure of 650 Pa and power of 40 W. The purpose of these latter measurements was to give information on the arrangement of Co and CoO regions in the composite "Co+CoO" layers. Such information could not be obtained trivially via GIXR (see below).

III. RESULTS AND DISCUSSION

A. Structural characterization

Representative specular (θ-2θ) x-ray reflectivity data from the multilayers are shown in Fig. 1(a). For multilayers with $t_{Ag}\lessapprox4$ nm, no well-defined Co+CoO/Ag bilayer (superlattice) Bragg peaks are present. Such peaks appear only in multilayers with $t_{Ag}\gtrapprox4$ nm.

Recently, we presented similar results to these—but for only one value of $t_{Ag}=4$ nm—in an article[13] dealing with the surfactant role played by oxygen in Ag sputter growth (see Fig. 3 in Ref. 13), where we attributed the absence of Bragg peaks for the case of sputtering in the absence of oxygen to the roughness of the Ag layers being comparable to the nominal thickness (in that case 1.3 nm) of the Co layers. However, considering now the results in Fig. 1(a) (this paper), where all samples were prepared with the same (nonzero) pressure of oxygen, it is physically implausible that the disappearance of the peaks for low t_{Ag} should be due to enhanced roughness since for a continuous layer, the roughness should certainly increase as some power law with the thickness (up to some cutoff[15]); this has been demonstrated for the case of vapor deposition of Ag onto silicon substrates for Ag film thicknesses above 10 nm.[16] A plausible explanation for the disappearance of the superlattice peaks, both in the previous and present works, would be a loss in true multilayer periodicity resulting from a transition from continuous to discontinuous Ag layers. This possibility is investigated below by means of in-plane resistivity measurements.

Figure 1(b) shows the Co+CoO/Ag bilayer thicknesses, $t_{bilayer}$, determined from the positions of the superlattice peaks present for $t_{Ag}\geqslant4$ nm. Subtracting the nominal Ag layer thickness (t_{Ag}) from $t_{bilayer}$ yields the thickness of the Co+CoO layer, t_{Co+CoO} (also plotted in the figure), which turns out to have a roughly constant value $\bar{t}_{Co+CoO}=(1.9\pm0.2)$ nm.

Representative x-ray diffractograms for the cases of $t_{Ag}>4$ nm and $t_{Ag}<4$ nm are shown in Fig. 1(c). The x-ray

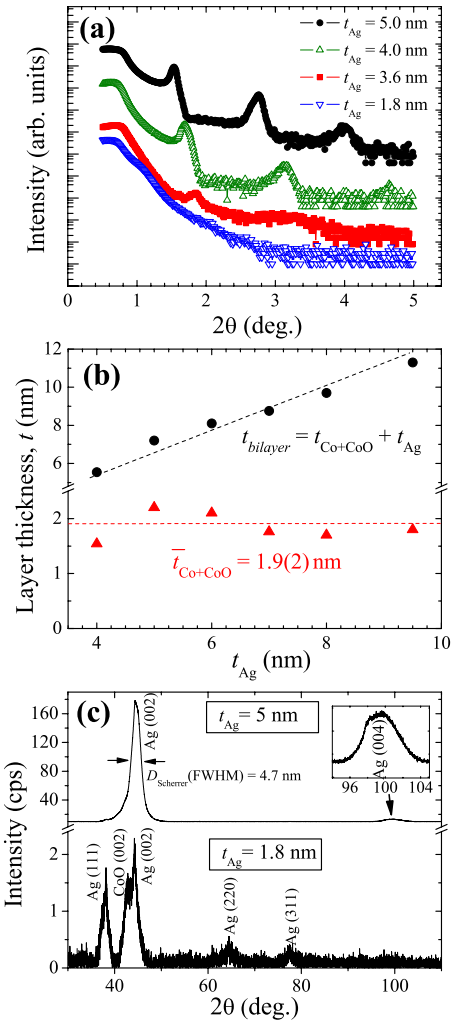

FIG. 1. (Color online) (a) Representative specular grazing incidence x-ray reflectivity across the t_{Ag} range and (b) the Co+CoO/Ag bilayer ($t_{bilayer}$) and Co+CoO layer (t_{Co+CoO}) thicknesses determined from the positions of the superlattice peaks for $t_{Ag}>4$ nm. (c) X-ray diffraction patterns for the minimum t_{Ag} value (=1.8 nm) and $t_{Ag}=5$ nm. The latter is representative of patterns for $t_{Ag}>4$ nm; the XRD evolves toward this from that for $t_{Ag}=1.8$ nm with increasing t_{Ag}.

diffraction (XRD) of the latter case ($t_{Ag}=1.8$ nm) evolves toward that of the former ($t_{Ag}=5$ nm) with increasing t_{Ag}. The (002) reflection of fcc CoO is detected for $t_{Ag}<4$ nm multilayers, whereas above 4 nm, the XRD patterns are dominated by ⟨002⟩ textured Ag, which overshadow any possible trace of ⟨111⟩ orientated fcc Co or CoO grains. Studies[13] on the sputter growth of Ag as a function of the oxygen pressure confirm that no Ag oxide phase is present for the working pressure in the present study (2×10^{-5} mbar). The Scherrer grain size of Ag (4.7 nm) determined by the width (full width at half maximum) of the (002) peak is consistent with the value of the Ag layer thickness for the $t_{Ag}=5$ nm sample.

Figure 2 shows the t_{Ag} dependence of the room temperature electrical resistivity, where it is observed that as $t_{Ag}\rightarrow4$ nm, the resistivity decreases, the multilayers becoming

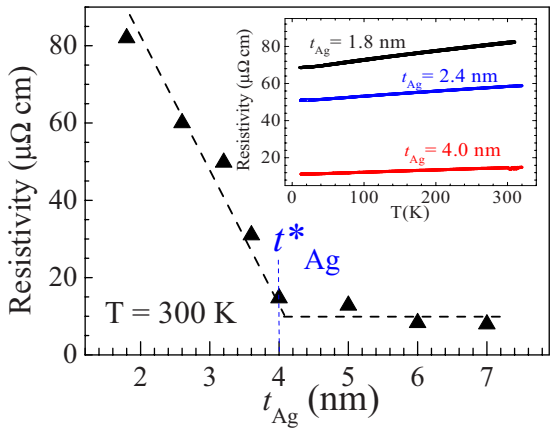

FIG. 2. (Color online) Room temperature electrical resistivity as a function of Ag layer nominal thickness, t_{Ag}. The blue dotted line marks the thickness, t^*_{Ag}, at which continuity is reached in the Ag layers. The inset shows representative resistivities as a function of temperature.

increasingly better conductors, while for $t_{Ag}>4$ nm, the resistivity of the multilayers is approximately constant. Since electron transport will mainly take place in the Ag layers (better conductors than the composite Co-CoO layers), it seems natural to identify the fall in resistivity as being due to the same transition from a discontinuous to a continuous film nature observed in sputter growth of Ag in the absence of oxygen,[11] but with a lower continuity limit, $t^*_{Ag}=4$ nm, due to the presence of oxygen in the sputtering chamber and its inherent surfactant effect.[13] An additional effect expected to accompany the transition to continuous Ag layers and lead, also, to a reduction in the resistivity is that of a reduction in the density of interfaces,[12] especially of type Co-Ag owing to spin dependent scattering (magnetoresistance) contributions.[17,18] Indeed, from the approximately constant resistivity for $t_{Ag}>t^*_{Ag}$, we may infer that the morphology of the Co-CoO composite layers essentially does not vary above t^*_{Ag}. This idea is supported by the following magnetic characterization.

Figures 3(a)–3(d) show hysteresis curves recorded at $T=300$ K over a range of values of t_{Ag} for two field orientations: parallel and perpendicular to the multilayer plane. The adjacent panels [(e)–(h)] show ZFC magnetization curves for the same values of t_{Ag}. Two main trends are observed in the data with increasing t_{Ag} ($\rightarrow t^*_{Ag}$): (i) the multilayers become increasingly anisotropic in terms of the magnetization response [(a)–(d)] and (ii) the peak in the ZFC curve [(e)–(h)], which indicates superparamagneticlike behavior (for T above that of the peak), progressively smears out.

The hysteresis curves [(a)–(d)] indicate a transition from a granular regime [samples containing FM (Co) particles with a relatively isotropic magnetic response] to a platelet regime (more extended FM regions in the plane, with a highly anisotropic response) as $t_{Ag}\rightarrow4$ nm ($=t^*_{Ag}$). A similar transition in the nature of sputter-deposited Co has been observed in studies of Ag/Co multilayers under variation of the Co nominal thickness.[17] The presence of a peak in the ZFC magnetization curve for $t_{Ag}=1.8$ nm [Fig. 3(e)] indicates a superparamagnetic behavior with an average blocking temperature

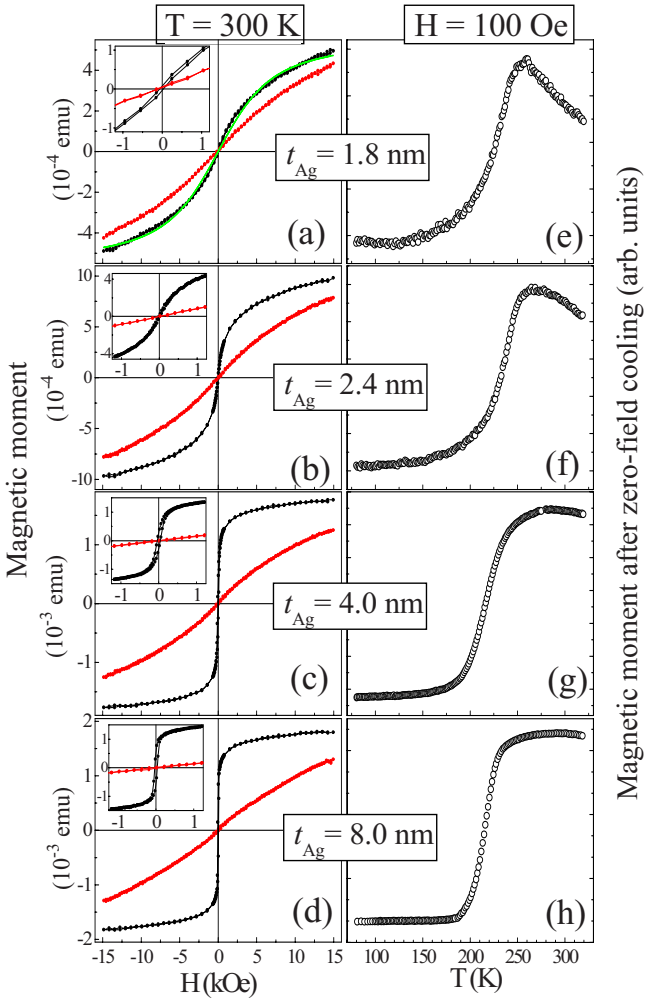

FIG. 3. (Color online) (a)–(d) Hysteresis curves recorded at 300 K with the magnetic field H applied parallel (black points) and perpendicular (red points) to the multilayer plane as a function of t_{Ag}: (a) 1.8 nm, (b) 2.4 nm, (c) 4.0 nm, and (d) 8.0 nm. The insets show close-ups of the low field region, showing that the coercive fields are very small. A fit using a Langevin function is shown by the green line in (a). (e)–(h) Zero-field-cooled (ZFC) magnetization curves measured with $H=100$ Oe (applied parallel to the multilayer plane) for t_{Ag} values corresponding to the adjacent hysteresis loops. The magnetic moment in all panels refers to the signal from a single multilayer.

signaled by the peak at $T_B=250$ K and points out the nanoscopic size of the FM regions in the granular regime. The peak is lost for $t_{Ag} \gtrapprox 4$ nm, i.e., the FM regions (Co platelets) present in these samples are large and/or anisotropic enough to be stable at 320 K (at least). In fact, the RT magnetic response for $t_{Ag}=1.8$ nm can be fitted reasonably well to a simple Langevin function [see panel (a)], yielding an effective particle moment of $1700\mu_B$ (corresponding to a mean particle diameter of particles of about 3 nm, assuming the bulk value for the Co atomic moment). Of course, this is only a very crude estimation—given the proximity of T_B to RT among other factors—but emphasizes the ultrafine size of the Co particles present in the granular multilayers as a result of the incomplete oxidation of the Co layers. This type of fit

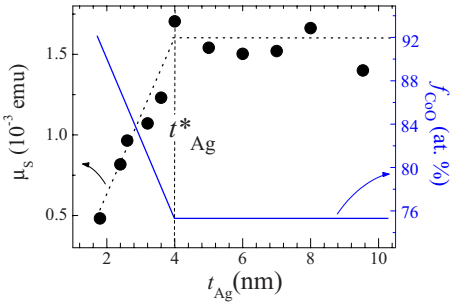

FIG. 4. (Color online) Saturation magnetic moment (at $T=300$ K) of the multilayers as a function of Ag layer nominal thickness, t_{Ag}. The dotted line through the points is a guide to the eye; the solid (blue) line shows the deduced variation in the CoO fraction, f_{CoO}. The vertical dashed line marks the thickness, t^*_{Ag}, at which continuity is reached in the Ag layers (Fig. 2).

becomes increasingly poor for thicker Ag layers and yields unrealistically large particle sizes (to be superparamagnetic at RT) for $t_{Ag}>4$ nm. Moreover, the increase of the ZFC magnetization for $t_{Ag}=1.8$ nm with increasing temperature from $T=80$ K [Fig. 3(e)] indicates the deblocking of progressively larger FM nanoparticles, i.e., a nanoparticle size distribution. The progression toward a temperature independent magnetization (below ~200 K) with increasing t_{Ag} may be explained on the basis of exchange coupling of the FM regions with AFM (CoO) regions, as will be discussed later.

Figure 4 shows the t_{Ag} dependence of the room temperature saturation magnetic moment extracted from hysteresis curves measured with H parallel to the sample plane [such as those in Figs. 3(a)–3(d)]. One observes an initial rise in the saturation magnetization with increasing t_{Ag} up to the continuity limit, t^*_{Ag} (Fig. 2), after which the magnetization appears constant. Given that an identical quantity of Co was deposited across the series of multilayers, the rise in magnetization may be explained by a reduction, as $t_{Ag} \rightarrow t^*_{Ag}$, in the fraction, f_{CoO}, of Co atoms that are oxidized (an increase in the fraction of FM Co, f_{Co}). Of course, strictly speaking, there is no reason for this oxide to be CoO, and any oxide which does not give rise to a FM component will suffice. However, this is the only oxide identified in XRD (see above). Since full oxidation of the deposited Co is never achieved across the multilayer series, and CoO is the least "oxygen-consuming" Co oxide, the presence of other oxides is not expected. The temperature dependence of EB properties (to be discussed later) provides further evidence for CoO. We have measured the saturation magnetic moment at room temperature of a Co/Ag multilayer (with $t_{Ag}>t^*_{Ag}$) grown in the absence of oxygen ($\mu_S=7\times10^{-3}$ emu) as a reference to estimate the variation in the fraction f_{Co} across the series. The y scale on the right hand side in Fig. 4 gives the f_{CoO} $(=1-f_{Co})$ values.

As a consistency check, we now calculate the thickness of the composite Co+CoO layers for the $t_{Ag}>t^*_{Ag}$ (continuous multilayer) regime using the corresponding estimated fractions of Co and CoO. The following relationship is expected to hold:

$$t_{\mathrm{Co+CoO}} = \left(f_{\mathrm{Co}} + \frac{v_{\mathrm{CoO}}}{v_{\mathrm{Co}}} f_{\mathrm{CoO}} \right) t_{\mathrm{Co}}^{nom},$$

where v_{Co} and v_{CoO} are, respectively, the effective volumes per Co atom in the Co and CoO phases (i.e., the unit cell volume divided by the corresponding number of Co atoms in the cell). For $t_{\mathrm{Ag}} > t_{\mathrm{Ag}}^{*}$, a value of $f_{\mathrm{Co}}=0.24$ ($f_{\mathrm{CoO}}=0.76$) has been estimated from the (average) saturation magnetic moment. This gives $t_{\mathrm{Co+CoO}}=1.9$ nm, in excellent agreement with the value ($\bar{t}_{\mathrm{Co+CoO}}$) determined by x-ray reflectivity [Fig. 1(b)].

The Co oxidation process is understood to be primarily due to the reactive atmosphere rather than to the adsorbed oxygen that will be present on the Ag surfaces (owing to the surfactant role of oxygen[13]). The role of the adsorbed oxygen, previously suggested to be important in the Co oxidation process,[19] has been found to be negligible based on measurements of the saturation magnetic moment of Co/Co "multilayer" samples prepared with an identical number of Co layers (each of $t_{\mathrm{Co}}^{nom}=1.2$ nm) as in the Co/Ag multilayers, again deposited in an oxygen atmosphere of pressure 2×10^{-5} mbar, and where a waiting time of 4 s between each layer deposition was employed, equivalent to the estimated exposure time to oxygen of each newly deposited Co layer prior to being effectively buried by the subsequent Ag layer in the preparation of the Co/Ag multilayers with $t_{\mathrm{Ag}} > t_{\mathrm{Ag}}^{*}$. These saturation magnetic moments (at room temperature) turned out to be very similar to that measured in Co/Ag multilayers with $t_{\mathrm{Ag}} > t_{\mathrm{Ag}}^{*}$.

Based on the information in Figs. 1–4, a plausible conjecture on the growth process of Co/Ag multilayers in an oxygen atmosphere of pressure of 2×10^{-5} mbar, where critically thin Co layer quantities (nominal thickness of 1.2 nm) are deposited each time but where the Ag layer thickness is varied from multilayer to multilayer, is as follows. For $t_{\mathrm{Ag}} < t_{\mathrm{Ag}}^{*}$ (=4 nm), the Ag layers are discontinuous [Figs. 1(a) and 2] and, as a result, the Co deposits as granules in the spaces between Ag islands, whereas for $t_{\mathrm{Ag}} > t_{\mathrm{Ag}}^{*}$, the Ag layers are continuous and, consequently, more continuous (plateletlike) Co regions are formed. Due to surface/volume ratio arguments, the Co granules oxidize more readily than the extended Co regions (Fig. 4). As $t_{\mathrm{Ag}} \rightarrow t_{\mathrm{Ag}}^{*}$, coalescence of Ag islands into larger regions results in an increase in the lateral dimension of Co granules (they become increasingly plateletlike) and, hence, a reduction in the surface:volume ratio of these particles, accounting for the decrease in f_{CoO} (Fig. 4). Once Ag continuity is established, the roughness of the Ag layer is expected to increase[16] upon further increase of t_{Ag}; however, this has a negligible effect on the subsequent Co oxidation process over the studied t_{Ag} range. Of course, the oxidation of Co will also take place in the path from the Co cathode to the substrate; however, the results presented here demonstrate the importance of the morphology (continuous or discontinuous nature) of the Ag in controlling the final oxide fraction.

A secondary question arising for the continuous regime concerns how the Co platelets are distributed within the Co+CoO layers in the direction perpendicular to the multilayer, i.e., whether, for example, the platelets are sandwiched by

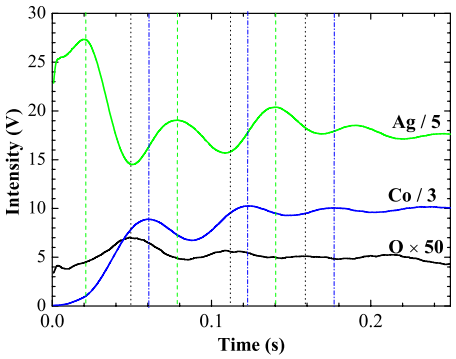

FIG. 5. (Color online) Glow discharge optical emission spectroscopy (GDOES) measurements on the multilayer with $t_{\mathrm{Ag}}=8$ nm. The signals from the three elemental components of the multilayer have been scaled in order to lie on the same y scale. The dotted, dashed, and dot-dashed lines mark the signal maxima for each element.

CoO or the oxide is mainly above or below. X-ray reflectivity simulations (not shown) demonstrate that it is difficult to distinguish with this technique between such possible Co+CoO morphologies occurring in Co/Ag multilayers. In order to gain some insight into the Co+CoO morphology, GDOES was undertaken, and typical results are shown in Fig. 5. The essential feature in the figure is the appearance of the peaks from oxygen prior to the Co peaks. From this, we infer that, within each Co+CoO layer, the CoO lies, on average, closer to the interface with the upper Ag layer than the Co. The overlap of elemental signals is mainly related to the sputtering process inherent to the technique, whereby a certain mixture of the signals from the walls and the base of the sputter-removed well takes place. As a means of summary, Fig. 6 illustrates the two general types of morphologies for the Co/Ag multilayers inferred from the results presented so far (Figs. 1–5).

B. Exchange-bias and related magnetic properties

Having established the structural changes occurring in the multilayers upon varying the Ag nominal thickness, we now present the EB properties of these systems. Figure 7 shows hysteresis curves measured at $T=80$ K after field cooling in $H=10$ kOe for four representative samples. The maximum magnetic moment of each multilayer has been normalized to unity to aid in the comparison of the forms of the different curves. We observe that with increasing t_{Ag}, a progressive increase in the coercive field (H_C) and a decrease in the loop shift (H_E) take place.

The dependence of H_E and H_C on t_{Ag} at $T=80$ K is shown in Figs. 8(b) and 8(c); caption (a) is a summary of results in Figs. 2 and 4. Two opposed behaviors are observed: H_E decreases while H_C increases as $t_{\mathrm{Ag}} \rightarrow t_{\mathrm{Ag}}^{*}$. For $t_{\mathrm{Ag}} > t_{\mathrm{Ag}}^{*}$, both parameters become roughly constant. One plausible effect which is capable of accounting for these behaviors is the following. That the decrease in f_{CoO} [Fig. 8(a)] concomitant with the change from a granular [Fig. 6(a)] to a platelet [Fig. 6(b)] Co regime is associated with a reduction in the *effective*

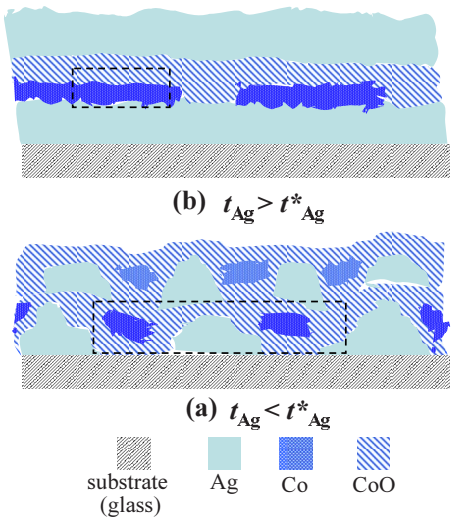

FIG. 6. (Color online) Schematics to show the deduced multilayer structure for the cases (a) $t_{Ag} < t^*_{Ag}$ (=4 nm), where Ag layers are discontinuous, and (b) $t_{Ag} > t^*_{Ag}$, where the Ag layers are continuous. In (a), the first four (i.e., Ag/Co/Ag/Co) layer depositions are depicted, whereas (b) shows the first three (Ag/Co/Ag). The box in (a) encloses two Co particles that have a combined volume equal to the volume of the Co platelet enclosed by the box in (b)—see discussion in text on the EB properties.

thickness of the AFM regions, t_{AFM} (where by "effective" we imply thicknesses measured in the directions perpendicular to the FM-AFM interfaces[9]). Via such an effect, the average anisotropy energy of the AFM regions, E_{AFM} ($\propto t_{AFM}$),[8] would reduce, (i) allowing spins in the AFM to be dragged more easily with the reversal of FM spins, thus leading to an enhancement in H_C, and (ii) producing a drop in the H_E because of the weaker pinning strength of such AFM spins.[8]

A decrease in the FM/AFM interface area per unit volume of Co is also expected to occur as $t_{Ag} \rightarrow t^*_{Ag}$ [see the boxes drawn in Fig. 6: each box contains an equivalent volume of Co but the platelet case, in (b), corresponds to the smaller interfacial area], which is capable[5,14] of accounting for a reduction in H_E but *not* a simultaneous increase in H_C. As a result, we believe such a mechanism to be secondary to the

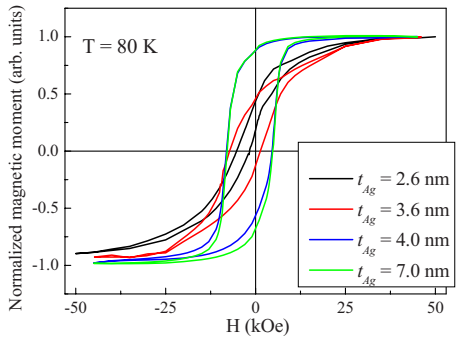

FIG. 7. (Color online) Hysteresis curves recorded at 80 K for selected values of t_{Ag} (with H parallel to the multilayer plane). The maximum magnetic moment has then been normalized to unity in each case.

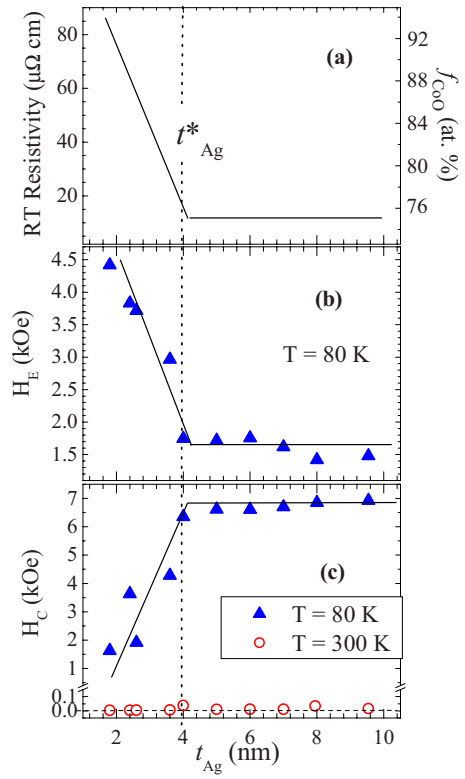

FIG. 8. (Color online) (a) A summary of results in Figs. 2 and 4: the development of continuity in the Ag layers (left axis) is associated with a fall in the CoO fraction (right axis). (b) and (c) Dependencies of the exchange-bias and coercive fields (both measured at 80 K) on the Ag layer nominal thickness, t_{Ag}, respectively. The solid lines are guides to the eye. The vertical dashed line marks the thickness, t^*_{Ag}, at which continuity is reached in the Ag layers. Also shown in (c) are the coercive fields measured at room temperature.

effect of a decrease in t_{AFM} in determining the $H_E(t_{Ag})$ dependence.

One might also expect an increased contribution to H_C from shape anisotropy as Co particles merge to form layer-like regions as $t_{Ag} \rightarrow t^*_{Ag}$. However, hysteresis loops recorded across the series at room temperature [examples of which are shown in Figs. 3(a)–3(d)] display similar H_C values, which are much less than those values observed at 80 K after FC—see open circles in Fig. 8(c). This demonstrates that coercivity at 80 K [Fig. 8(c)] is due to exchange coupling.

The smallest EB fields (for $t_{Ag} > t^*_{Ag}$) which have been measured are still relatively large ($\approx$1.5 kOe), bearing in mind the very small value of t_{AFM} [we estimate an average of just 1.5 nm for the CoO layer sketched in Fig. 6(b)]. In a recent study by Nogués *et al.*[6] on Co-CoO core-shell particles, with t_{AFM} similar to that deduced for $t_{Ag} > t^*_{Ag}$, embedded in Al_2O_3, highly degraded EB properties (EB onset temperatures $T_{OE} < 100$ K and $H_E < 200$ Oe) were observed for low particle two-dimensional coverages (yielding negligible particle-particle connectivity). The EB properties of the multilayers studied here indicate higher stability of the AFM regions compared to those core-shell systems, which is assumed to be provided by connectivity in the discontinuous (Ag) regime and by the layer geometry in the continuous (Ag) regime.

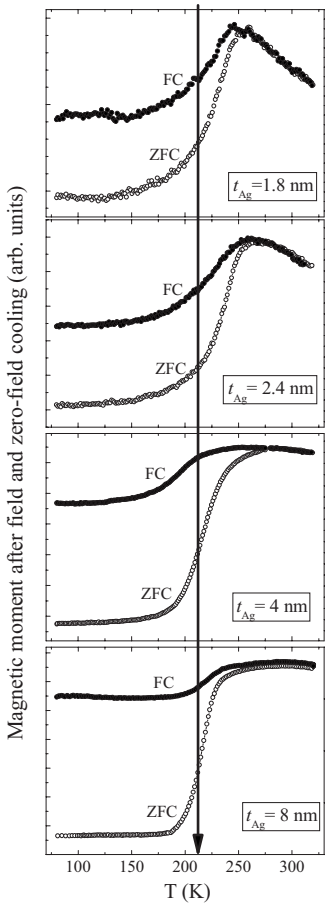

FIG. 9. Field-cooled (FC) (closed points) and zero-field-cooled (ZFC) (open points) magnetization curves. The vertical line marks the estimated EB onset temperature.

The temperature dependencies of the ZFC magnetization below ~200 K [Figs. 3(e)–3(h)] are now discussed. These results are replotted in Fig. 9, along with FC magnetization curves. The vertical line in the figure marks the EB onset temperature (T_{OE}), which has been estimated from hysteresis loops measured up to a maximum field of 10 kOe at temperatures just above and just below 220 K, after heating from the field-cooled state (see Sec. II). The same value of onset temperature may be assigned to the entire series of multilayers, $T_{OE} \approx 210$ K, i.e., above this temperature, the loops become centered in the applied field axis. It is worth noting that just below T_{OE} (e.g., $T=200$ K), where a loop displacement in the H axis may be detected, the hysteresis loops (with $H_{max}=10$ kOe) are *closed* and centered in the y axis. This allows us to eliminate minor hysteresis loop effects[20] in our estimation of T_{OE}.

In the granular samples [Figs. 9(a) and 9(b)], the ZFC magnetization increases gradually upon heating until it reaches a well-defined maximum at $T_B \approx 250$ K, whereas in the continuous multilayers, the ZFC magnetization is nearly constant at low temperatures and then increases abruptly to reach a higher value plateau when the exchange anisotropy becomes vanishingly small at approximately 210 K. These features can be explained in terms of the magnetic domain structures expected from the sample morphologies sketched in Fig. 6. The ZFC curve of the granular samples is certainly typical of superparamagnets, the decrease above T_B indicating the existence of very small ($\lesssim 5$ nm) unconnected FM regions [Fig. 6(a)]. The shape of the FC magnetization indicates strong interparticle interactions (as in superspin glasses[21,22]). On the other hand, the temperature dependence of the ZFC magnetization for the continuous (Ag) multilayers can be explained as follows. When the sample is zero field cooled through the Néel temperature, AFM domains are formed, the configuration of which is influenced by the domain structure of the adjacent, unmagnetized Co platelet through exchange coupling, so that Co domains are effectively pinned when a small magnetic field ($H=100$ Oe) is applied at a low temperature. This scenario explains the flatness of the curve up to temperatures where the exchange coupling vanishes (at $T_{OE} \approx 210$ K), and the magnetic domains unpin. The flatness of both curves (ZFC and FC) above T_{OE} indicates the presence of FM regions (Co platelets) of sizes large and/or anisotropic enough to be thermally stable at room temperature. As a final note, the value of T_{OE} of all the samples (around 210 K) is similar to that observed in a variety of Co-CoO systems with thicker AFM layers,[8,23,24] which serves as an additional piece of evidence for the AFM oxide to be CoO.

IV. CONCLUSIONS

Upon varying the nominal thickness, t_{Ag}, of the Ag layers in sequentially, reactively sputter-deposited Co/Ag, we have observed a dramatic change in the morphological and, consequently, the EB properties of the magnetic layers across the series of multilayers. Two regimes are observed: in the first ($t_{Ag} < t^*_{Ag}=4$ nm), electrical transport and magnetic parameters (magnetization and exchange-bias and coercive fields) of the multilayers strongly depend on t_{Ag}, whereas in the second ($t_{Ag} > t^*_{Ag}$), all parameters become essentially t_{Ag} independent. The crossover between the two regimes is related to the continuity transition, at t^*_{Ag}, in the silver layers. For $t_{Ag} < t^*_{Ag}$, a granular morphology is induced in the Co deposits, which in turn leads to a higher degree of oxidation compared to deposition onto continuous Ag layers (i.e., $t_{Ag} > t^*_{Ag}$), where Co deposits acquire a platelet (more continuous) nature. These conclusions are supported by a series of experimental pieces of evidence: electrical resistivity data (reflecting the development of continuity in the Ag layers), which exactly mimics the variation of the fraction of CoO with t_{Ag} (as extracted from the saturation magnetic moments)—see Figs. 2, 4, and 8(a); the development of an increasingly anisotropic magnetic response of the multilayers as $t_{Ag} \to t^*_{Ag}$, coupled with the loss of the peak in the ZFC magnetization measurements, where superparamagnetic behavior (i.e., the presence of fine Co particles) is observed only for $t_{Ag} < t^*_{Ag}$ (Fig. 3); and x-ray reflectivity studies, where the "true" multilayer structure [i.e., Co+CoO/Ag superlattice (bilayer) Bragg peaks in specular curves] is observed only for $t_{Ag} > t^*_{Ag}$ [Fig. 1(a)]. In addition, glow discharge optical emission spectroscopy (Fig. 5) shows spatially separated peaks from silver, oxygen, and cobalt for the last few deposited layers for multilayers with $t_{Ag} > t^*_{Ag}$. A reduc-

tion in the effective thickness of the AFM regions may explain the behavior in both H_E and H_C as $t_{Ag} \rightarrow t^*_{Ag}$, this thickness being expected to be larger in the proposed granular morphology [Fig. 6(a)] than in the continuous (Ag) one [Fig. 6(b)]. A secondary possible factor is the FM/AFM interface area per unit quantity of Co, which should be larger in the granular morphology and contribute to the change in H_E only. Finally, our study provides information on the surfactant role played by oxygen in the Ag sputter growth[13] since the value of the continuity limit found here (t^*_{Ag}=4 nm) is significantly lower than the value found (≈6 nm) in previous studies of Ag sputter deposition in the absence of oxygen.[11,12]

ACKNOWLEDGMENTS

We acknowledge financial support from the JCLM (Project No. GC-02-009) and the Ministerio de Educación y Ciencia (P.S.N., SB 2004-0071). We thank M. Rivera and E. Prado for their expert technical support in the preparation of the multilayer samples.

[1] V. Skumryev, S. Stoyanov, Y. Zhang, G. Hadjipanayis, D. Givord, and J. Nogués, Nature (London) **423**, 850 (2003).
[2] J. M. Riveiro, J. A. De Toro, J. P. Andrés, J. A. González, T. Muñoz, and J. P. Goff, Appl. Phys. Lett. **86**, 172503 (2005).
[3] A. N. Dobrynin *et al.*, Appl. Phys. Lett. **87**, 012501 (2005).
[4] C. Portemont, R. Morel, A. Brenac, and L. Notin, J. Appl. Phys. **100**, 033907 (2006).
[5] P. S. Normile, J. A. De Toro, J. P. Andrés, J. A. González, T. Muñoz, P. Muñiz, A. J. Barbero, and J. M. Riveiro, J. Appl. Phys. **100**, 064312 (2006).
[6] J. Nogués, V. Skumryev, J. Sort, S. Stoyanov, and D. Givord, Phys. Rev. Lett. **97**, 157203 (2006).
[7] W. H. Meiklejohn and C. P. Bean, Phys. Rev. **102**, 1413 (1956); **105**, 904 (1957).
[8] J. Nogués, J. Sort, V. Langlais, V. Skumryev, S. Suriñach, J. S. Muñoz, and M. D. Baró, Phys. Rep. **422**, 65 (2005).
[9] M. S. Lund, W. A. A. Macedo, K. Liu, J. Nogués, I. K. Schuller, and C. Leighton, Phys. Rev. B **66**, 054422 (2002).
[10] C. Binek, A. Hochstrat, and W. Kleemann, J. Magn. Magn. Mater. **234**, 353 (2001).
[11] S. E. Paje, F. Teran, J. M. Riveiro, J. Llopis, M. A. Garcia, M. de Lucas, and L. Saviot, Mater. Sci. Forum **480**, 287 (2005).
[12] J. Milano, A. M. Llois, L. B. Steren, A. Butera, and J. Barnard, J. Appl. Phys. **96**, 7392 (2004).
[13] J. M. Riveiro, P. S. Normile, J. P. Andrés, J. A. González, J. A. De Toro, T. Muñoz, and P. Muñiz, Appl. Phys. Lett. **89**, 201902 (2006).
[14] J. A. De Toro, J. P. Andrés, J. A. González, P. Muñiz, T. Muñoz, P. S. Normile, and J. M. Riveiro, Phys. Rev. B **73**, 094449 (2006).
[15] A.-L. Barabási and H. E. Stanley, *Fractal Concepts in Surface Growth* (Cambridge University Press, New York, 1995).
[16] C. Thompson, G. Palasantzas, Y. P. Feng, S. K. Sinha, and J. Krim, Phys. Rev. B **49**, 4902 (1994).
[17] R. Lololee, P. A. Schroeder, W. P. Pratt, Jr., J. Bass, and A. Fert, Physica B **204**, 274 (1995).
[18] F. Fettar, L. B. Steren, A. Barthélémy, R. Morel, A. Fert, J. A. Barnard, and J. D. Jarratt, J. Magn. Magn. Mater. **165**, 316 (1997).
[19] T. Muñoz, J. A. De Toro, P. S. Normile, J. P. Andrés, J. A. González, P. Muñiz, A. J. Barbero, and J. M. Riveiro, J. Appl. Phys. **101**, 09E504 (2007).
[20] J. Geshev, J. Magn. Magn. Mater. (to be published).
[21] D. L. Peng, K. Sumiyama, T. Hihara, S. Yamamuro, and T. J. Konno, Phys. Rev. B **61**, 3103 (2000).
[22] J. A. De Toro, M. A. Lopez de la Torre, J. M. Riveiro, A. Beesley, J. P. Goff, and M. F. Thomas, Phys. Rev. B **69**, 224407 (2004).
[23] S. Gandopadhyay, G. C. Hadjipanayis, C. M. Sorensen, and K. J. Klabunde, J. Appl. Phys. **73**, 6965 (1993).
[24] J. B. Tracy, D. N. Weiss, D. P. Dinega, and M. G. Bawendi, Phys. Rev. B **72**, 064404 (2005).